Lattice Bhatnagar-Gross-Krook models for miscible fluids

E. G. Flekkøy
Department of Physics, University of Oslo, Box 1048 Blindern, 0316 Oslo, Norway
(Received 16 July 1992)

Lattice Bhatnagar-Gross-Krook models for miscible fluid flow in two (2D) and three (3D) dimensions are introduced. The convection-diffusion (CD) equation and the Navier-Stokes (NS) equation describing the macroscopic behavior of the models are derived using the Chapman-Enskog expansion technique. Corrections to the CD equation of higher order in the flow velocity are obtained, and it is shown how the present models are linked with the existing Boltzmann model. It is also shown how the Navier-Stokes dynamics is explicitly decoupled from the diffusive behavior of the model. The results obtained from both 2D and 3D simulations are observed to be in excellent agreement with the analytic predictions. In particular it is shown that the models are well described by theory for high-Péclet-number flows. We also present simulation results confirming the anomalous (but small) velocity dependence of the CD equation, and we investigate the models' sensitivity to large gradients in the concentration profile.

PACS number(s): 68.10.−m, 47.10.+g, 02.70.−c, 51.10.+y

INTRODUCTION

Since the first lattice-gas automaton (LGA) for the simulation of two-dimensional (2D) fluid dynamics was introduced by Frisch, Hasslacher, and Pomeau [1] in 1986, a rich variety of related cellular automaton-type models have appeared.

The original model is a genuine cellular automaton relying on a fully discretized picture of a fluid. Particles move on a triangular lattice and are only allowed to interact at the lattice nodes. Every time step thus contains a movement (streaming) and a collision part. When the collisions satisfy mass and momentum conservation it can be shown that the lattice gas develops macroscopic dynamics which is very close to incompressible Navier-Stokes behavior. The macroscopic dynamics is obtained by taking either spatial or time averages of the particle velocities.

Since the updating rules are strictly local and very simple, the introduction of complex boundaries is a simple matter. The model has been successfully applied to simulations of flow in porous media [2]. The LGA is a microscopic model in the sense that the fluid flow may be viewed as an averaged flow of interacting particles. Due to this natural physical interpretation the LGA is easily extended to deal with a number of phenomena that are more complicated than incompressible single phase flow. There exist extensions of the model that deals with miscible [3,4] and immiscible [5] fluid flow, flow with temperature variations [6], and osmotic flow across semipermeable membranes [7].

In the LGA model particles are represented by single-bit occupation numbers $n_i(\mathbf{x},t) = 0$ or 1, corresponding to the presence or absence respectively of a particle at the position $\mathbf{x}$ at time t with velocity in the direction labeled i. Thus, information about 32 particles can be stored in a single computer word. This property was called *bit democracy* by von Neumann since every bit contains the same amount of information. It makes the model very memory efficient, and, since there are no roundoff errors involved in single-bit manipulations, numerical stability is guaranteed. However, the inherent statistical fluctuations require a large amount of averaging in order to obtain smoothly varying macroscopic quantities.

In order to avoid these fluctuations the lattice Boltzmann (LB) models [8] use the mean occupation numbers $N_i = \langle n_i \rangle$ instead of the occupation numbers themselves, as the basic quantities. The algorithms for these models are given by the Boltzmann equation which describes the time evolution of the distribution functions of LGA model. There is a tradeoff, however, between the absence of noise in the hydrodynamic quantities and memory efficiency, because the N_i's need to be represented by 32 bits each.

Both the LGA and the LB models suffer from some deficiencies that are due to the exclusion principle (there can be at most one particle in a given direction at a given site) and the discreteness of the velocities: The Navier-Stokes equation describing the models contains an anomalous prefactor in the convection term, which therefore breaks Galilean invariance [9], and the pressure term depends on the flow velocity. Also, in the LGA and LB models the viscosity is determined by the choice of collision rules. This restricts these models to a rather limited range of Reynolds numbers. This constraint is removed in the linearized lattice Boltzmann (LLB) model first introduced by Higuera and co-workers [10–12], where it is observed that the collision operator can be linearized around a local equilibrium, and need not correspond to the detailed choice of collision rules of the LGA, as long as it conserves mass and momentum. Contrary to the LB model this model is also easily extended to 3D. In both the LGA and the (L)LB models the isotropy of the hydrodynamic equations is due to the structure of the underlying lattice. In 2D simulations the lattice is triangular whereas in 3D a projection of the 4D face centered

hypercubic lattice [13] must be used.

Recently Qian, d'Humiéres, and Lallemand [14] proposed an alternative to the lattice Boltzmann models called lattice Bhatnagar-Gross-Krook (BGK) models [15]. In these models isotropy is ensured through the particular choice of equilibrium values for the average occupation numbers N_i, and simple cubic lattices are used. The equilibrium distribution functions are chosen to recover Galilean invariance and to remove the velocity dependence in the pressure term. The collision step is reduced to a multiplication by a relaxation parameter whereas a full collision matrix with the same rank as the number of directions on the lattice is employed in the LLB models. Compared with the LGA, from which the lattice Boltzmann models evolved, the BGK models represent a further abstraction of the original model. The collision operator of the LLB models may be constructed to correspond to a specific choice of collision rules in the LGA. This is not the case for the BGK models. However, the conservation of mass and momentum, necessary to obtain hydrodynamic behavior, is kept in the collision step of the BGK models.

During recent years several models for two-phase flow have been introduced. A linearized lattice Boltzmann model corresponding to the original lattice-gas model for immiscible fluids [5] exists due to Gunstensen *et al.* [16]. Recently a linearized 2D lattice Boltzmann model for miscible fluids was introduced by Holme and Rothman [17].

In this paper we propose BGK models for miscible fluid flow in both 2D and 3D. Keeping the algorithmic simplicity of the BGK models as well as the extra richness associated with having two fluids, these models rely on a combination of the ideas of both Holme and Rothman, and Qian, d'Humiéres, and Lallemand. The two relaxation parameters of the models may be identified with the eigenvalues of the LLB collision operator corresponding to the transport of color and momentum.

To apply these models to the simulation of realistic systems it is often necessary to work at high Reynolds or Peclet numbers. This can be achieved in one of two ways: either by using large lattices, and thereby a large amount of computational resources, or by performing the simulations with small transport coefficients. The latter strategy is clearly preferable, and in the model of Holme and Rothman, as well as in the present models, the transport coefficients are continuously tunable parameters. However, the use of small transport coefficients will support large gradients in the corresponding hydrodynamic quantities. If these quantities develop detailed structure on a scale below the cutoff given by the lattice constant, the models will fail to produce physical results. This is a problem inherent to all numerical models where the physical space is represented by a discrete lattice. The lattices must therefore be large enough to sample the relevant fields with a close enough spacing.

The 3D model employs the cubic lattice with 15 velocity directions on each node as used by Qian, d'Humiéres, and Lallemand. However, for the sake of direct comparison with the existing Boltzmann model, the 2D model is implemented using the same triangular lattice as the Frisch-Hasslacher-Pomeau (FHP) models. Using the triangular lattice for the 2D model, the velocity dependence in the pressure is still present. As shown by Qian, d'Humiéres, and Lallemand, this could be avoided by using a different lattice.

The fluids are distinguished as either "red" or "blue." The basic variables of the models are the distribution functions

$$N_i = R_i + B_i \ , \tag{1}$$

$$\Delta_i = R_i - B_i \ , \tag{2}$$

where R_i (B_i) is the mean occupation number for red (blue) particles in direction i at a given node. This choice of variables decouples the information on mass density and flow (N_i) from the information on the relative amount of color (Δ_i) in the sense that the time evolution of the N_i's is independent of the Δ_i's. Thus, the fluid dynamics, as seen by a colorblind observer, is the same as in the models proposed by Qian, d'Humiéres, and Lallemand [14]. The diffusive behavior of the mixing fluids is superimposed on the underlying Navier-Stokes dynamics.

Although the convection diffusion equation describing these models has been derived within the context of the LGA [3], an analysis of the corrections to this equation due to terms of higher order in the flow velocity seems to be lacking. At a high Peclet number, when the diffusive transport of color is small compared to the convective transport, these corrections are potentially of crucial importance. However, it is shown in this paper that they are proportional to D, and hence do not dominate even when D is small.

For the models to be well described by theory the corresponding systems must be in a state of local equilibrium. We derive the time of relaxation to local equilibrium as a function of the transport coefficients and show how the transients may be removed by initializing the distribution functions with a dependence on the gradients in the conserved quantities (color and momentum).

A comparison between the present BGK models and the Boltzmann model proposed by Holme and Rothman is given, and it is shown how the latter may be reduced to the former by a proper decomposition of the collision operator. In both models a large amount of the computation time is consumed by the calculation of the equilibrium distributions, which is done at every node at every time step. However, the simplification represented by the BGK models becomes particularly clear in 3D. The collision step of the BGK model consists of a multiplication by two parameters, whereas the Boltzmann model would require a multiplication by a 48×48 collision matrix.

The simulations were performed in the high-Péclet-number (low diffusion constant) regime and the results show good agreement with theory.

THE MODELS AND THEIR FLUID DYNAMIC EQUATIONS

We will derive the macroscopic equations for the color densities and, for the sake of completeness, briefly review how the corresponding Navier-Stokes equations for

mass and momentum densities are obtained [14]. A detailed derivation of the Navier-Stokes equations within the context of the LGA models can be found in Ref. [9], and it has also been derived by Qian, d'Humiéres, and Lallemand [14] within the context of the BGK models.

The starting point will be the Boltzmann equations [9] which describe the time evolution of the distribution functions. Since these equations obey color and momentum conservation, the macroscopic equations follow from a (Chapman-Enskog) expansion in the gradients of the conserved densities. The 2D model will in the following be referred to as the FHP model because of its triangular lattice whereas, conforming to the terminology of Qian, d'Humiéres, and Lallemand, the 3D model will be referred to as the D3Q15 (3 dimensions, 15 velocities) model.

The updating scheme is contained in the Boltzmann equations

$$N_i(\mathbf{x}+\mathbf{c}_i, t+1) = N_i(\mathbf{x},t) + \lambda_\nu\, N_i^{\mathrm{neq}}(\mathbf{x},t), \tag{3}$$

$$\Delta_i(\mathbf{x}+\mathbf{c}_i, t+1) = \Delta_i(\mathbf{x},t) + \lambda_D\, \Delta_i^{\mathrm{neq}}(\mathbf{x},t), \tag{4}$$

where λ_ν and λ_D are the relaxation parameters which determine the kinematic viscosity ν and the diffusion coefficient D, respectively. Within the context of the FHP model these parameters will be identified with the eigenvalues of the linearized collision operator corresponding to the color and momentum current, respectively. The nonequilibrium distributions are given as

$$\begin{aligned} N_i^{\mathrm{neq}} &= N_i - N_i^{\mathrm{eq}}, \\ \Delta_i^{\mathrm{neq}} &= \Delta_i - \Delta_i^{\mathrm{eq}}, \end{aligned} \tag{5}$$

where

$$N_i^{\mathrm{eq}} = t_i\rho(1 + c_s^{-2}\mathbf{u}\cdot\mathbf{c}_i + GQ_{i\alpha\beta}u_\alpha u_\beta), \tag{6}$$

$$\Delta_i^{\mathrm{eq}} = t_i\Delta\rho(1 + c_s^{-2}\mathbf{u}\cdot\mathbf{c}_i). \tag{7}$$

Here the mass density per site is defined as

$$\rho = \sum_i N_i \tag{8}$$

and the momentum density as

$$\rho\mathbf{u} = \sum_i \mathbf{c}_i N_i\ . \tag{9}$$

The density difference $\Delta\rho = \rho_r - \rho_b$, where ρ_r (ρ_b) is the site density of red (blue) particles, is defined as

$$\Delta\rho = \sum_i \Delta_i\ . \tag{10}$$

The vectors $\mathbf{c}_i$ are the velocity vectors on the lattice connecting neighboring nodes. On the triangular lattice they all have unit length. On the cubic lattice one of the $\mathbf{c}_i$'s have zero length, the eight $\mathbf{c}_i$'s connecting nearest neighbors have unit length, and the six velocities connecting next nearest neighbors have length $\sqrt{3}$. The speed of sound [18] $c_s = 1/\sqrt{2}$ for the FHP model and $c_s = 1/\sqrt{3}$ for the D3Q15 model. The t_i's are chosen to obtain isotropy of the fourth-order velocity moments and depend only on the lengths of the $\mathbf{c}_i$'s. For the FHP model $t_i = 1/6$, and for the D3Q15 model,

$$t_i = \begin{cases} \frac{2}{9} & \text{when } |\mathbf{c}_i| = 0 \\ \frac{1}{9} & \text{when } |\mathbf{c}_i| = 1 \\ \frac{1}{72} & \text{when } |\mathbf{c}_i| = \frac{1}{\sqrt{3}}. \end{cases} \tag{11}$$

The G factor will reappear in the prefactor of the convection term of the Navier-Stokes equation. For Galilean invariance to hold this prefactor must equal one. The corresponding values for G are 4 and 4.5 for the FHP model and BGK models, respectively. The tensor $Q_{i\alpha\beta}$ is given by

$$Q_{i\alpha\beta} = c_{i\alpha}c_{i\beta} - c_s^2\delta_{\alpha\beta}, \tag{12}$$

where α and β are Cartesian indices and $\delta_{\alpha\beta}$ is the Kronecker delta function.

Every update of the lattice is thus a three-step process: First the equilibrium distributions are calculated from the above expressions. Then the collision step, given by the multiplication by λ_D and λ_ν in Eqs. (3) and (4), is performed before, finally, the occupation numbers are propagated to the neighboring sites.

We will need the following relations:

$$\begin{aligned} \sum_i t_i &= 1, \\ \sum_i t_i\mathbf{c}_i &= 0, \\ \sum_i t_i Q_{i\alpha\beta} &= 0, \end{aligned} \tag{13}$$

which are derived in Refs. [9] and [14]. The first relation gives the normalization of the equilibrium distributions. The second relation is a consequence of the parity symmetry of the lattice. Due to this symmetry all odd-order velocity moments vanish. The last of the above relations can be viewed as a completeness relation.

The time and spatial dependence of the equilibrium distributions appear through the hydrodynamic densities only. It should be observed that Δ_i^{eq} contains no second-order terms in u. This second-order term must be included in the N_i's in order to get the convection term in the Navier-Stokes equation. But since the convection diffusion equation contains no second-order velocity terms, Δ_i^{eq} can be of first order in u.

The convection diffusion equation

The nonequilibrium terms defined in Eq. (5) represent the response in the distribution functions to gradients in the macroscopic densities $\Delta\rho$, ρ, and $\mathbf{u}$. Using the relations (13) it is seen that

$$\sum_i \Delta_i^{\mathrm{eq}} = \Delta\rho \tag{14}$$

and therefore

$$\sum_i \Delta_i^{\text{neq}} = 0 \,. \tag{15}$$

By summing Eq. (4) over i it is seen that conservation of color can be expressed as

$$\sum_i [\Delta_i(\mathbf{x}+\mathbf{c}_i, t+1) - \Delta_i(\mathbf{x}, t)] = 0 \,. \tag{16}$$

We will derive the continuity and convection diffusion equations from Eq. (16) using the multiscale Chapman-Enskog expansion [9]. This is an expansion of the distribution functions in the gradients of the conserved quantities. It relies on the assumption that the lattice may be set up with a scale separation between the scale of spatial variations in $\Delta\rho$, defined as ϵ^{-1}, and the lattice constant. It is also assumed that $|\mathbf{u}|$ varies on the same scale ϵ^{-1}. This means that

$$\begin{aligned} &\partial_\alpha \Delta\rho \sim \epsilon, \\ &|\partial_\alpha \mathbf{u}| \sim \epsilon, \end{aligned} \tag{17}$$

where ∂_α is the derivative with respect to x_α. A two-time formalism is used, i.e., we set

$$\partial_t = \partial_{t_1} + \partial_{t_2} \,. \tag{18}$$

This splitting in two time scales, as done in Ref. [9], is really not necessary to obtain the transport equations. It can be viewed merely as a convenient (and instructive) way of dividing the expansion procedure in two steps. The final results are obtained by summing the equations containing ∂_{t_1} and ∂_{t_2}, respectively. We assume that

$$\begin{aligned} &\partial_{t_1} \mathbf{u} = \mathbf{0}, \\ &\partial_{t_2} \mathbf{u} \sim \epsilon^2 \mathbf{u}, \\ &\partial_{t_1} \Delta\rho \sim \epsilon, \\ &\partial_{t_2} \Delta\rho \sim \epsilon^2, \end{aligned} \tag{19}$$

This implies that there are no rapid time variations in the velocity field. This is the same assumption that is made in the derivation of the incompressible Navier-Stokes equation. There, however, it is also required to assume that $|\mathbf{u}| \sim \epsilon$. For the present derivation we will keep all orders in u and we must therefore allow for rapid variations in the color field due to convection. We will assume that we are in the incompressible regime, i.e., that

$$\boldsymbol{\nabla} \cdot \mathbf{u} = 0 \,. \tag{20}$$

The first continuity equation follows from an expansion to first order in ϵ. Performing a Taylor expansion of Eq. (16) around $(\mathbf{x}, t)$ we get

$$\sum_i (\mathbf{c}_i \cdot \boldsymbol{\nabla} + \partial_{t_1}) \Delta\rho^{\text{eq}} = 0, \tag{21}$$

where higher order terms in ϵ are neglected, and where we have used that $\Delta_i^{\text{neq}} \sim \epsilon$ since Δ_i^{neq} is a function only of the gradients in $\Delta\rho$ and $\mathbf{u}$. Using the relations (13) and substituting from Eq. (7), the above equation reduces to

$$\partial_{t_1} \Delta\rho + \boldsymbol{\nabla} \cdot (\Delta\rho \mathbf{u}) = 0 \,. \tag{22}$$

This continuity equation expresses what was anticipated above: that rapid variations in $\Delta\rho$ are due to convection. From Eq. (20) it is seen that Eq. (22) also takes the form

$$\partial_{t_1} \Delta\rho + \mathbf{u} \cdot \boldsymbol{\nabla} \Delta\rho = 0 \,. \tag{23}$$

In order to obtain the diffusive contribution to the transport of color, corresponding to the slower time dependence, we need to go to second order in ϵ. For this Δ_i^{neq} must be determined. When the system has reached local equilibrium this can be done directly from the Boltzmann equation (4), which gives

$$\Delta_i^{\text{neq}} = \frac{1}{\lambda_D} (\mathbf{c}_i \cdot \boldsymbol{\nabla} + \partial_{t_1}) \Delta_i^{\text{eq}} \tag{24}$$

to first order in ϵ. On the right-hand side Δ_i has been replaced by Δ_i^{eq}, since Δ_i^{neq} is itself of $O(\epsilon)$.

We now proceed to collect all the terms of Eq. (16) that are of second order in ϵ. This gives

$$\sum_i \partial_{t_2} \Delta_i^{\text{eq}} + \sum_i (\mathbf{c}_i \cdot \boldsymbol{\nabla} + \partial_{t_1}) \Delta_i^{\text{neq}} + \sum_i \tfrac{1}{2} (\mathbf{c}_i \cdot \boldsymbol{\nabla} + \partial_{t_1})^2 \Delta_i^{\text{eq}} = 0, \tag{25}$$

where the last term is the second-order term in the Taylor expansion. Inserting the expression for Δ_i^{neq} given in Eq. (24) and using Eqs. (14) and (15), the above equation takes the form

$$\partial_{t_2} \Delta\rho + \left(\frac{1}{2} + \frac{1}{\lambda_D}\right) \sum_i (\mathbf{c}_i \cdot \boldsymbol{\nabla} + \partial_{t_1})^2 \Delta_i^{\text{eq}} = 0. \tag{26}$$

Using Eqs. (13) and (20), and Eq. (23) to replace time derivatives with spatial derivatives, we obtain

$$\partial_{t_2} \Delta\rho = D_0 (\nabla^2 \Delta\rho - c_s^{-2} (\mathbf{u} \cdot \boldsymbol{\nabla})^2 \Delta\rho), \tag{27}$$

where we have introduced the diffusion coefficient

$$D_0 = -c_s^2 \left(\frac{1}{\lambda_D} + \frac{1}{2}\right) \tag{28}$$

as in Ref. [17]. Adding Eqs. (23) and (27) to obtain the full time dependence in $\Delta\rho$, we get

$$(\partial_t + \mathbf{u} \cdot \boldsymbol{\nabla}) \Delta\rho = D_0 (\nabla^2 \Delta\rho - c_s^{-2} (\mathbf{u} \cdot \boldsymbol{\nabla})^2 \Delta\rho) \,. \tag{29}$$

This is the convection diffusion equation with the required velocity corrections. It expresses conservation of the quantity $\Delta\rho = \rho_r - \rho_b$. Supplemented with the conservation of the mass density $\rho = \rho_r + \rho_b$ conservation of the density difference is seen to be equivalent to conservation of the individual amounts of red and blue. Moreover, in the low Mach number regime ρ is essentially constant, so derivatives of $\Delta\rho$ in Eq. (29) can be replaced by twice the derivatives of ρ_r or ρ_b.

The validity of the convection diffusion equation in the

form above is limited by the incompressibility and scale assumptions, as is the validity of the Navier-Stokes equation. The last term in Eq. (29) breaks Galilean invariance. But this symmetry breaking will be very weak since u must be small in order to stay in the regime where the incompressibility assumption holds. Being proportional to u^2 the last term will typically represent only a 1% correction. The important feature of Eq. (29) is that the velocity correction terms are multiplied by the diffusion constant D_0, hence they do not dominate when D_0 is small.

The Navier-Stokes equation

We now turn to the derivation of the Navier-Stokes equation. The scale assumptions made in this case is that u and ρ have spatial variations on the scale ϵ^{-1} and time variations on the scale ϵ^{-2}. It is also assumed that the flow velocity itself is small, i.e., $u \sim \epsilon$, and that deviations in ρ from its average value is also of the order ϵ. These assumptions can be written as

$$\begin{aligned} &\partial_\alpha u \sim \epsilon u \sim \epsilon^2, \\ &\partial_t u \sim \epsilon^3, \\ &\partial_\alpha \rho \sim \epsilon^2, \\ &\partial_t \rho \sim \epsilon^3 . \end{aligned} \tag{30}$$

Observing that

$$\begin{aligned} &\sum_i N_i^{\mathrm{eq}} = \rho \\ &\sum_i \mathbf{c}_i N_i^{\mathrm{eq}} = \rho \mathbf{u} , \end{aligned} \tag{31}$$

which implies that

$$\sum_i N_i^{\mathrm{neq}} = \sum_i \mathbf{c}_i N_i^{\mathrm{neq}} = 0 , \tag{32}$$

it is seen that the Boltzmann equation (3) conserves mass and momentum, i.e.,

$$\sum_i N_i(\mathbf{x} + \mathbf{c}_i, t+1) - N_i(\mathbf{x}, t) = 0, \tag{33}$$

$$\sum_i \mathbf{c}_i (N_i(\mathbf{x} + \mathbf{c}_i, t+1) - N_i(\mathbf{x}, t)) = 0 . \tag{34}$$

Following exactly the same lines as in the derivation of the transport equations for color, the continuity equation (20) may be derived from an order-ϵ^2 expansion of Eq. (33), and the incompressible Navier-Stokes equation from an order ϵ^3 expansion of Eq. (34). In this case $o(\epsilon^2)$ is the lowest order expansion of Eqs. (33) and (34) which are nontrivial. The $o(\epsilon^2)$ expansion of Eq. (34) gives

$$\nabla \rho = \mathbf{0} . \tag{35}$$

For the $o(\epsilon^3)$ expansions of Eqs. (33) and (34) we need to determine N_i^{neq} to $o(\epsilon^2)$. As with Δ_i^{neq} this can be done directly from Eq. (3), which gives

$$N_i^{\mathrm{neq}} = \frac{1}{\lambda_\nu} (\mathbf{c}_i \cdot \nabla + \partial_t) N_i^{\mathrm{eq}} . \tag{36}$$

With this result at hand the third-order expansions of Eqs. (33) and (34) can be derived in the same way as the convection diffusion equation. To this order Eq. (33) simply gives

$$\partial_t \rho = 0 . \tag{37}$$

This means that deviations in ρ from its average value must be smaller than first order in ϵ. The Navier-Stokes equation emerges from the third-order expansion of the momentum conservation relation (34). Performing this expansion using Eqs. (13), (20), (35), and (37), we get

$$\begin{aligned} &\rho \partial_t u_\alpha + G \rho T_{\alpha\beta\gamma\delta} \partial_\beta u_\gamma u_\delta \\ &\quad = -c_s^2 \partial_\alpha \rho - c_s^{-2} \left(\frac{1}{\lambda_\nu} + \frac{1}{2} \right) \rho T_{\alpha\beta\gamma\delta} \partial_\beta \partial_\gamma u_\delta, \end{aligned} \tag{38}$$

where $T_{\alpha\beta\gamma\delta}$ is defined [19] as

$$T_{\alpha\beta\gamma\delta} = \sum_i t_i c_{i\alpha} c_{i\beta} Q_{i\gamma\delta} . \tag{39}$$

It can be shown [9, 20] that this tensor is isotropic and takes the following form:

$$T_{\alpha\beta\gamma\delta} = \begin{cases} \frac{1}{8} \left(\delta_{\alpha\gamma}\delta_{\beta\delta} + \delta_{\alpha\delta}\delta_{\beta\gamma} - \frac{2}{D}\delta_{\alpha\beta}\delta_{\gamma\delta} \right) & \text{for the FHP model} \\ \frac{1}{9} \left(\delta_{\alpha\gamma}\delta_{\beta\delta} + \delta_{\alpha\delta}\delta_{\beta\gamma} \right) & \text{for the D3Q15 model.} \end{cases} \tag{40}$$

Inserting these formulas in Eq. (38), we obtain the incompressible Navier-Stokes equation

$$\partial_t \mathbf{u} + (\mathbf{u} \cdot \nabla)\mathbf{u} = -\frac{1}{\rho} \nabla P + \nu \nabla^2 \mathbf{u}, \tag{41}$$

where the kinematic viscosity is given as

$$\nu = \begin{cases} -\frac{1}{4} \left(\frac{1}{\lambda_\nu} + \frac{1}{2} \right) & \text{for the FHP model} \\ -\frac{1}{3} \left(\frac{1}{\lambda_\nu} + \frac{1}{2} \right) & \text{for the D3Q15 model.} \end{cases} \tag{42}$$

When λ_ν is identified as the eigenvalue of the collision operator corresponding to transport of momentum, this

is the result obtained in Ref. [9]. The pressure is given as

$$P = \begin{cases} \frac{1}{2}\rho(1-u^2) & \text{for the FHP model} \\ \frac{1}{3}\rho & \text{for the D3Q15 model.} \end{cases} \tag{43}$$

This is the equation of state of the gas. The velocity correction in the FHP version of the Navier-Stokes equation coming from the pressure term is small, like the corresponding correction in the convection diffusion equation. It stems from the last term in the expression for the $T_{\alpha\beta\gamma\delta}$ tensor given in Eq. (40). As Qian, d'Humiéres, and Lallemand shows, it can be removed by a proper choice of velocities, $\mathbf{c}_i$'s, and normalization factors t_i's.

The approach to local equilibrium

The superscript (neq) labeling the parts of the distribution functions that are due to the gradients in the macroscopic quantities refers to the fact that the system is evolving in time towards a homogeneous steady state. However, when the distribution functions are initialized with their equilibrium values (or any arbitrary values), there will also be a development towards a local equilibrium characterized by the expressions given for the nonequilibrium distributions in Eqs. (24) and (36). There are thus two types of equilibria: the local equilibrium that depends on the size of the gradients and the overall, thermodynamic, equilibrium which has no time development. The system must reach local equilibrium before it will behave according to the macroscopic equations obtained, and the time scale for the approach to local equilibrium must therefore be much smaller than the hydrodynamic time scale on which overall equilibrium is approached.

We will now obtain the time dependence of the distribution functions when they are initialized with their equilibrium values. This will also give the stability criteria of the model in terms of the relaxation parameters λ_ν and λ_D.

For the sake of simplicity we consider the situation where there is a constant color gradient, vanishing flow velocity, and constant density ρ. The distribution functions are initialized with their equilibrium values given by Eqs. (6) and (7), and the color gradient is maintained at a constant value by suitable boundary conditions. We will consider only the time variation in Δ_i since the N_i's will keep their equilibrium values.

With the assumptions made above, we may assume that the equilibrium part of Δ_i depends only on $\mathbf{x}$, and that the nonequilibrium part depends only on t and λ_D. Therefore, from Eq. (4) we may write

$$\Delta_i^{\text{neq}}(\lambda_D, t+1) = (1+\lambda_D)\Delta_i^{\text{neq}}(\lambda_D, t) - [\Delta_i^{\text{eq}}(\mathbf{x}+\mathbf{c}_i) - \Delta_i^{\text{eq}}(\mathbf{x})]. \tag{44}$$

Performing a Taylor expansion of the last term and substituting from Eq. (7), we obtain the recursion relation

$$\Delta_i^{\text{neq}}(\lambda_D, t+1) = (1+\lambda_D)\Delta_i^{\text{neq}}(\lambda_D, t) - t_i\mathbf{c}_i\cdot\boldsymbol{\nabla}\Delta\rho(\mathbf{x}) . \tag{45}$$

This relation gives, upon iteration, the full time dependence

$$\begin{aligned}\Delta_i^{\text{neq}}(\lambda_D, t) &= -\sum_{n=0}^{t-1}(1+\lambda_D)^n t_i\mathbf{c}_i\cdot\boldsymbol{\nabla}\Delta\rho(\mathbf{x}) \\ &= [1-(1+\lambda_D)^t]\left(\frac{t_i}{\lambda_D}\mathbf{c}_i\cdot\boldsymbol{\nabla}\Delta\rho(\mathbf{x})\right),\end{aligned} \tag{46}$$

where we have used that $\Delta_i^{\text{neq}}(\lambda_D, 0) = 0$. The last factor may be recognized as the value of Δ_i^{neq} given in Eq. (24). It is seen that Δ_i^{neq} will converge to the value given by Eq. (24) only when

$$\lambda_D \in (-2, 0) . \tag{47}$$

A typical time scale for the decay of transients is given by the quantity

$$t_* = \frac{-1}{\ln|1+\lambda_D|} . \tag{48}$$

When D is small (and λ_D is close to -2) we have

$$t_* \approx \frac{1}{2+\lambda_D} . \tag{49}$$

This means that for low diffusivities, t_* might approach the hydrodynamic time scale and the system fails to produce physical results. In order to avoid this, the distribution functions may be initialized with their predicted dependence on gradients as given in Eqs. (24) and (35). A closed form for the nonequilibrium distributions is obtained using (23) to replace time derivatives with spatial derivatives. This gives

$$N_i^{\text{neq}} = \frac{t_i}{\lambda_\nu}\rho c_s^{-2} Q_{i\alpha\beta}\,\partial_\alpha u_\beta, \tag{50}$$

$$\Delta_i^{\text{neq}} = \frac{t_i}{\lambda_D} c_s^{-2}(Q_{i\alpha\beta}\,\partial_\beta(\Delta\rho u_\beta) - (u_\alpha u_\beta - c_s^2\delta_{\alpha\beta})c_{i_\alpha}\partial_\beta\Delta\rho). \tag{51}$$

The gradients in the conserved quantities must be computed as finite differences prior to the initialization.

The above analysis is easily extended to more general situations. In particular, by introducing nonvanishing gradients in the velocity field, results for the evolution of the N_i's, which are exactly similar to those given in Eq. (46), can be obtained. The stability condition on λ_ν is

$$\lambda_\nu \in (-2, 0) \tag{52}$$

as shown in Ref. [14].

THE CONNECTION WITH THE BOLTZMANN MODEL

Having analyzed the BGK models we now establish the connection with the existing Boltzmann model [17]. We show how the collision operator of this model may be decomposed to make explicit the decoupling between the N_i's and the Δ_i's. We also derive the second-order velocity corrections to the transport equations describing the

Boltzmann model and compare with those of the BGK model.

In order to simplify the algebra and some of the conceptual points we introduce a bra-ket notation for vectors with components labeled by the direction index i. The Boltzmann FHP model works with the 12-vector

$$|Y\rangle = (R_1, B_1, R_2, B_2, \ldots, R_6, B_6)^t \,, \tag{53}$$

where R_i and B_i are the mean occupation numbers for red and blue, respectively, and t denotes the transpose. The collision part of the algorithm is given as

$$|Y(\mathbf{x}, t_+)\rangle = |Y(\mathbf{x}, t)\rangle + \Omega |Y^{\rm neq}\rangle, \tag{54}$$

where t_+ denotes the time after collision, but before propagation, Ω is the 12×12 collision matrix, and $|Y^{\rm neq}\rangle$ is calculated from the equilibrium distributions,

$$R_i^{\rm eq} = \frac{\rho_r}{6}\left(1 + 2\mathbf{u}\cdot\mathbf{c}_i + 4Q_{i\alpha\beta}u_\alpha u_\beta\right), \tag{55}$$

$$B_i^{\rm eq} = \frac{\rho_b}{6}\left(1 + 2\mathbf{u}\cdot\mathbf{c}_i + 4Q_{i\alpha\beta}u_\alpha u_\beta\right) \,. \tag{56}$$

The quantities ρ_r and ρ_b are the site densities of red and blue, and the rest of the notation is as defined above. The streaming step is performed in the ordinary way as described in Eqs. (3) and (4). The collision operator is given as

$$\Omega = \begin{pmatrix} \omega_0 & \omega_{60} & \omega_{120} & \omega_{180} & \omega_{120} & \omega_{60} \\ \omega_{60} & \omega_0 & \omega_{60} & \omega_{120} & \omega_{180} & \omega_{120} \\ \omega_{120} & \omega_{60} & \omega_0 & \omega_{60} & \omega_{120} & \omega_{180} \\ \omega_{180} & \omega_{120} & \omega_{60} & \omega_0 & \omega_{60} & \omega_{120} \\ \omega_{120} & \omega_{180} & \omega_{120} & \omega_{60} & \omega_0 & \omega_{60} \\ \omega_{60} & \omega_{120} & \omega_{180} & \omega_{120} & \omega_{60} & \omega_0 \end{pmatrix}, \tag{57}$$

where the indices on the 2×2 matrices ω are the angles between different lattice directions. We will also use the notation ω^i where $i = 0, 1, \ldots, 5$, and the relation $\omega^{6-i} = \omega^i$ reflects the isotropy of the collisions. The above matrix is seen to be block circulant [17,21], which, by definition, means that it can be written as

$$\Omega = \sum_{i=0}^{5} \Gamma^i \otimes \omega^i, \tag{58}$$

where Γ^i is the 6×6 matrix performing a circular leftshift by i places and $\otimes$ denotes the direct product.

In the work of Holme and Rothman, the action of ω^i on the pair $(R_i, B_i)^t$ is required to reduce to a scalar multiplication when the two colors are summed to give the noncolored occupation number N_i. If this is the only requirement that is made, Ω may be constructed to give the red and blue phases different viscosities. We also impose that the interaction between red and blue particles be symmetric. In that case ω^i is constrained to be of the form

$$\omega^i = \begin{pmatrix} r^i & s^i \\ s^i & r^i \end{pmatrix} \,. \tag{59}$$

The two different fluids may still be given different viscosities by making λ_ν a function of the relative concentration. With the above form of ω^i the collision matrix Ω is both real and symmetric and thus possesses a complete set of orthonormal eigenvectors. The ω^i's have the eigenvectors

$$|\chi_\pm\rangle = \frac{1}{\sqrt{2}}\begin{pmatrix} 1 \\ \pm 1 \end{pmatrix} \tag{60}$$

with corresponding eigenvalues $\alpha_\pm^i = r^i \pm s^i$. Since these eigenvectors are independent of ω^i the collision operator given in Eq. (58) may be written as

$$\Omega = \Omega^+ \otimes |\chi_+\rangle\langle\chi_+| + \Omega^- \otimes |\chi_-\rangle\langle\chi_-|, \tag{61}$$

where the 6×6 matrices $\Omega^\pm$ are given as

$$\Omega^\pm = \sum_{i=0}^{5} \alpha_\pm^i \Gamma^i \,. \tag{62}$$

Inserting this expression for the collision operator in Eq. (54), we get

$$|Y(\mathbf{x}, t_+)\rangle = |Y(\mathbf{x}, t)\rangle + \frac{1}{\sqrt{2}}\left(\Omega^+ |N^{\rm neq}\rangle \otimes |\chi_+\rangle + \Omega^- |\Delta^{\rm neq}\rangle \otimes |\chi_-\rangle\right), \tag{63}$$

where the definitions given in Eqs. (1) and (2) have been used. Taking the projection of the above equation on $|\chi_+\rangle$ and $|\chi_-\rangle$, respectively, we obtain an explicit decoupling between the mass and color information:

$$|N(\mathbf{x}, t_+)\rangle = |N(\mathbf{x}, t)\rangle + \Omega^+ |N^{\rm neq}\rangle, \tag{64}$$

$$|\Delta(\mathbf{x}, t_+)\rangle = |\Delta(\mathbf{x}, t)\rangle + \Omega^- |\Delta^{\rm neq}\rangle \,. \tag{65}$$

It can be shown that all the shift matrices Γ^j have common eigenvectors

$$|v_k\rangle = (1, \Lambda_k, \Lambda_{2k}, \ldots, \Lambda_{5k})^t \tag{66}$$

with corresponding eigenvalues Λ_{jk} where $\Lambda_k = e^{i\frac{2\pi}{6}k}$. The orthogonal set of vectors $|v_k\rangle$, $k = 0, 1, \ldots, 5$, are thus eigenvectors of $\Omega^\pm$ as well, with eigenvalues

$$\gamma_\pm^k = \sum_{j=0}^{5} \alpha_\pm^j \Lambda_{jk} \,. \tag{67}$$

It can be shown from the above equation that the relation $\omega^{6-i} = \omega^i$ must also hold for these eigenvalues:

$$\gamma_\pm^{6-k} = \gamma_\pm^k \,. \tag{68}$$

Being real and symmetric $\Omega^\pm$ can be written in terms of its eigenvectors as

$$\Omega^\pm = \frac{1}{6}\sum_{k=0}^{5} \gamma_\pm^k \, |v_k\rangle\langle v_k|, \tag{69}$$

where $\frac{1}{6}$ is a normalization factor. Equation (68) gives the only constraint on the eigenvalues $\gamma_\pm^k$, and there are thus four eigenvalues that can be chosen independently for each of the two collision operators.

The linear combinations of the vectors $|v_k\rangle$ given in Table I form an alternative orthogonal set of eigenvectors to $\Omega^{\pm}$ with a natural physical interpretation. The vector $|v_0\rangle$ is denoted $|m\rangle$ since it projects out the mass density ρ from $|N\rangle$ (and the density difference $\Delta\rho$ from $|\Delta\rangle$). The vectors $|c_\alpha\rangle$ and $|Q_{\alpha\beta}\rangle$ can be seen to have the components c_{i_α} and $Q_{i\alpha\beta}$, respectively. When the inner product of $|N\rangle$ and $|\Delta\rangle$ is formed with $|c_\alpha\rangle$ the mass and color currents are obtained. The vectors $|Q_{\alpha\beta}\rangle$ give the momentum transport when combined with $|N\rangle$ while $|v_3\rangle$ seems to have no obvious physical interpretation. Since $|Q_{12}\rangle = |Q_{21}\rangle$ and $|Q_{22}\rangle = -|Q_{11}\rangle$ the full set of $|Q_{\alpha\beta}\rangle$ are represented above.

It is customary to set the eigenvalues λ_m, λ_p, and λ_C equal to zero, thus ensuring that the collision operator conserves mass, momentum, and color. This, however, is not really necessary since, by construction, $|N^{\rm neq}\rangle$ has no components along $|v_0\rangle$ and $|c_{i_\alpha}\rangle$, and $|\Delta^{\rm neq}\rangle$ has no components along $|v_0\rangle$. The eigenvalues λ_2 and $\lambda_3^{\pm}$ are often set equal to -1 in order to remove the corresponding (unphysical) components in $|N\rangle$ and $|\Delta\rangle$.

The Boltzmann collision operator will reduce to the scalar multiplication of the BGK models if all the eigenvalues of Ω^+ are set equal to λ_ν and all the eigenvalues of Ω^- are set equal to λ_D.

The derivation of the convection diffusion equation is very similar to that given in the previous section. The first-order continuity equation (23) is exactly the same, whereas the convection diffusion equation receives velocity corrections which are slightly different due to the different choice of equilibrium distributions.

To second order in ϵ, Eq. (16) takes the form

$$\partial_{t_2}\langle v_0|\Delta^{\rm eq}\rangle + \langle c_\alpha\partial_\alpha + v_0\partial_{t_1}|\Delta^{\rm neq}\rangle + \tfrac{1}{2}\langle (c_\alpha\partial_\alpha + v_0\partial_{t_1})\odot(c_\alpha\partial_\alpha + v_0\partial_{t_1})|\Delta^{\rm eq}\rangle = 0, \quad (70)$$

where we have introduced the product $\odot$, defined as the multiplication component by component of two vectors to form a third vector of the same dimension, and $\langle\,|\,\rangle$ denotes the ordinary inner product corresponding to the summation over i in Eq. (16). Note that since $|\Delta^{\rm neq}\rangle$ is orthogonal to $|v_0\rangle$ we need only determine the product $\langle c_\alpha|\Delta^{\rm neq}\rangle$. A first-order Taylor expansion of the Boltzmann equation (65) gives

$$(|c_\alpha\rangle\partial_\alpha + |v_0\rangle\partial_{t_1})\odot|\Delta^{\rm eq}\rangle = \Omega^-|\Delta^{\rm neq}\rangle\,. \quad (71)$$

TABLE I. Eigenvectors and corresponding eigenvalues to the collision operators Ω^+ and Ω^-.

Eigenvector	Eigenvalue of Ω^+	Eigenvalue of Ω^-
$\|m\rangle = \|v_0\rangle$	λ_m	λ_C
$\|c_1\rangle = \frac{1}{2}(\|v_1\rangle + \|v_5\rangle)$	λ_p	λ_D
$\|Q_{11}\rangle = \frac{1}{4}(\|v_2\rangle + \|v_4\rangle)$	λ_ν	λ_2
$\|v_3\rangle$	λ_3^+	λ_3^-
$\|Q_{12}\rangle = \frac{1}{4i}(\|v_2\rangle - \|v_4\rangle)$	λ_ν	λ_2
$\|c_2\rangle = \frac{1}{2i}(\|v_1\rangle - \|v_5\rangle)$	λ_p	λ_D

Taking the inner product of this equation with $\langle c_\alpha|$ and letting Ω^- act to the left, we obtain

$$\langle c_\alpha|\Omega^-|\Delta^{\rm neq}\rangle = \lambda_D\langle c_\alpha|\Delta^{\rm neq}\rangle = \langle c_\alpha|\{(|c_\alpha\rangle\partial_\alpha + |v_0\rangle\partial_{t_1})\odot|\Delta^{\rm eq}\rangle\}. \quad (72)$$

Thus, substituting the expression for $\langle c_\alpha|\Delta^{\rm neq}\rangle$ given from the above equation in Eq. (70), we obtain

$$\partial_{t_2}\Delta\rho + \left(\frac{1}{2} + \frac{1}{\lambda_D}\right)\partial_\alpha\langle c_\alpha|(|c_\alpha\rangle\partial_\alpha + |v_0\rangle\partial_{t_1})\odot|\Delta^{\rm eq}\rangle = 0 \quad (73)$$

which is exactly the same as Eq. (26) except for the presence of the terms of second order in the velocity in $|\Delta^{\rm eq}\rangle$. The convection diffusion equation now takes the form

$$(\partial_t + \mathbf{u}\cdot\boldsymbol{\nabla})\Delta\rho = D_0\nabla^2(\Delta\rho(1-u^2)), \quad (74)$$

where $D_0 = -\frac{1}{2}\left(\frac{1}{\lambda_D} + \frac{1}{2}\right)$ as before.

It follows from Eq. (70) that, since only the components of $|\Delta^{\rm neq}\rangle$ along $|c_\alpha\rangle$ enter the transport equation, the eigenvalues λ_C, λ_2, and λ_3^- do not influence the hydrodynamic or diffusive behavior of the model.

The Navier-Stokes equation describing the Boltzmann model is the same as that describing the (2D) BGK model. The components of $|N^{\rm neq}\rangle$ that enter the Navier-Stokes equation are those along $|Q_{\alpha\beta}\rangle$, and therefore the only eigenvalue of Ω^+ that is relevant for the macroscopic behavior is λ_ν.

When the transport coefficients D and ν are small the relaxation time to local equilibrium will be controlled by the parameters λ_D and λ_ν. The relaxation time should therefore not be seriously affected by choosing all the eigenvalues of Ω^+ and Ω^- equal to λ_D and λ_ν, respectively.

SIMULATIONS

The simulations were performed in order to verify the theory presented in the previous sections, and to establish the practical limits of the model. We determine the diffusion coefficient D as a function of the control parameter λ_D by measuring the relaxation of a sinusoidal concentration wave both at rest and moving with a flow velocity u. The predicted u^2 dependence in the convection diffusion equation (29) is verified and the response to large gradients in the concentration field is examined.

The simulations were performed on a Connection Machine (CM2) with 32 768 processors and a memory of about 1 GByte distributed among the processors. The speed is 1.25 and 0.84 million site updates per second for the two- and three-dimensional models, respectively. The three-dimensional model will use about two-thirds of the memory when run on a 128^3 lattice. A flow simulation with a lattice of this size in which the fluids traverse the system at a speed $u = 0.1$ will consume less than 1 CPU hour. The models thus seem to lend themselves to rather large-scale simulations. For the present simulations, however, the lattice size was chosen so as to give one processor per lattice site when a fourth of the

Connection Machine was used. The models were implemented on this machine in order to make future applications possible, even though an ordinary workstation would have been sufficient for the present simulations.

Instead of working with $\Delta\rho(\mathbf{x},t)$ we use the relative concentration of red defined as

$$C_r = \frac{\rho_r}{\rho} = \frac{\Delta\rho+\rho}{2\rho} . \tag{75}$$

When ρ is constant C_r satisfies the convection diffusion equation. In the case that u is a constant as well the convection diffusion equation may be written

$$(\partial_t + \mathbf{u}\cdot\boldsymbol{\nabla})C_r = D\nabla^2 C_r, \tag{76}$$

where the effective diffusion coefficient is given as

$$D = (1 - c_s^{-2}u_{||}^2)D_0 , \tag{77}$$

and $u_{||}$ is the component of u parallel to the concentration gradient. We note that a solution of this equation, describing a decaying sine wave flowing along in the x direction with velocity u, is given as

$$C_r(\mathbf{x},t) = C_{\max}\,\tfrac{1}{2}(e^{-k^2Dt}\sin kx' + 1) , \tag{78}$$

where $x' = x - ut$. The diffusion coefficient can be computed from the decay of the area $A(t)$ enclosed by the x axis and the curve of the function

$$|C_r(x,t) - \tfrac{1}{2}C_{\max}| = \tfrac{1}{2}e^{-Dk^2t}|\sin kx'| . \tag{79}$$

It is easily shown that

$$D = \frac{1}{k^2t}\ln\left(\frac{A(0)}{A(t)}\right) . \tag{80}$$

This is the expression used to determine D from the simulations. Due to the periodic boundary conditions the area $A(t)$ is very well approximated by a simple Riemann sum. The system was initialized with $C_{\max} = 1$ and the lattice sizes used were 128×64 and $128 \times 64 \times 1$ in two and three dimensions, respectively [22].

We focus attention on the low diffusivity behavior of the model, which means that we examine a part of the parameter space where the model is on the border of being numerically unstable. A practical problem associated with this is that roundoff errors become important: When D is small the change in $C_r(x,t)$ due to diffusion is calculated from small differences between numbers of the order unity.

Figure 1 shows the diffusion coefficients D from both models as functions of λ_D when $u = 0$. The agreement between theory and simulations is seen to be excellent for values of D down to 10^{-4}. For lower values of D roundoff errors become significant when single precision numbers are used, and we observe deviations between theory and simulations of the order 10% when $D = 10^{-5}$. With double precision, however, the deviations become very small: At $D = 10^{-4}$ agreement between theory and simulation is within 0.02%. For the largest values of D the wave number k was chosen so that the wavelength equaled the x dimension of the lattice. For the smaller values

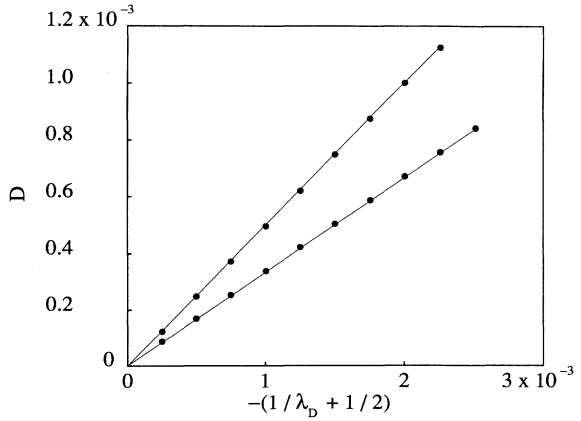

FIG. 1. The diffusion coefficient D as a function of $-(1/\lambda_D + 1/2)$, where λ_D is the relaxation parameter governing the evolution of Δ_i. The upper and lower graphs show results from 2D and 3D simulations, respectively. The dots represent results from simulations whereas the solid lines show the analytic values given in Eq. (28).

of D, however, the simulations were performed with an increasing number of waves in order to obtain a quicker decay and more accurate measurements of the change in the concentration profile. In the simulations we initialized the distribution functions with their nonequilibrium parts given in Eqs. (50) and (51). The gradients were obtained from the relation

$$\sum_i \mathbf{c}_i[\Delta_i(\mathbf{x},t) - \Delta_i(\mathbf{x}-\mathbf{c}_i,t)] \approx c_s^2\nabla\Delta\rho . \tag{81}$$

The calculation of the left-hand side is an easy matter when the streaming routine, which is used to perform the movement part of the algorithm, is used to derive the precollision distributions $\Delta_i(\mathbf{x}-\mathbf{c}_i,t)$ from $\Delta_i(\mathbf{x},t)$.

Figure 2 shows the concentration profile as a function

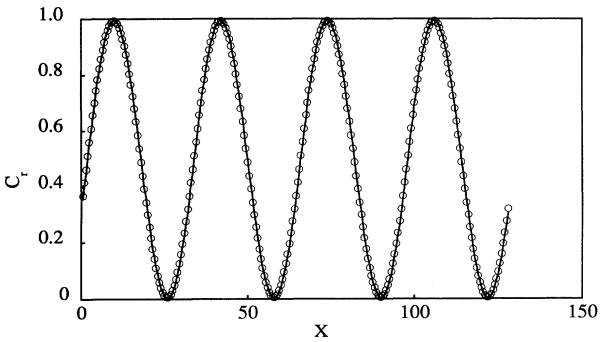

FIG. 2. The relative concentration of red $C_r(x,t)$, obtained from the 2D model, shown as a function of position x after $t = 220$ time steps. The flow velocity is $u = 0.15$ and the fluid has thus moved a distance of 33 lattice constants. The dots represent simulation results whereas the solid line show the analytic values for $C_r(x,t)$ given by Eq. (78) with $D = 1.20 \times 10^{-3}$ obtained from Eq. (77).

of the position x after a time $t = 220$ at a flow velocity $u = 0.15$. The solid curve shows the theoretical prediction from Eqs. (78) and (77). The circles show the simulation values. With the orientation of the lattice used, where one lattice direction is parallel to the x axis, it is possible to sample two values of C_r per unit length. In Fig. 2 there are thus 256 points.

In Fig. 3 the velocity dependence in the effective diffusion coefficient D given in Eq. (77) is compared with simulations. The simulated values of D are obtained through the formula given in Eq. (80). The agreement is seen to be good also for values of u which must be assumed to lie outside the Navier-Stokes regime.

It is of considerable interest to estimate the available Peclet numbers for the models. The Peclet number, Pe, measuring the ratio of convective to diffusive transport, is defined as

$$\mathrm{Pe} = \frac{uL}{D}, \tag{82}$$

where L is a length that is characteristic of the flow. It is seen from Fig. 3 that by setting $u = 0.15$ and $D = 10^{-3}$ we are well within the regime where the model is adequately described by theory. Taking L to be the lattice dimension, and setting $L = 1024$ and $L = 128$ for the 2D and 3D models, respectively, we get the following estimates:

$$\mathrm{Pe} \sim \begin{cases} 10^5 \text{ in 2D} \\ 10^4 \text{ in 3D.} \end{cases} \tag{83}$$

We also observed excellent agreement between simulations and theory for D as a function of λ_D for a flow velocity $u_y = 0.2$ perpendicular to the color gradient. In that case the velocity corrections vanish.

In Fig. 4 D is shown as a function of the maximum value of $\nabla\Delta\rho(x,t)$. These values are obtained by increasing the number of waves from one to 32. Single precision was used and deviations from theory due to roundoff errors are observed for small values of $(\nabla\Delta\rho)_{\max}$, when

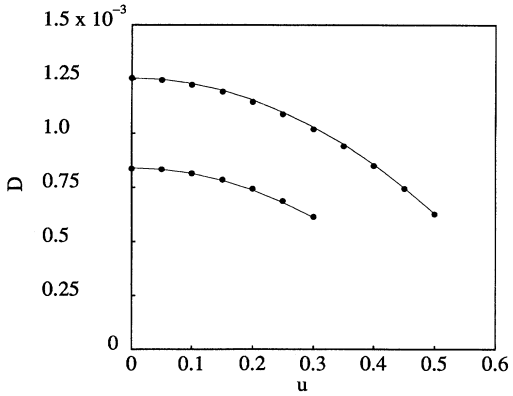

FIG. 3. The effective diffusion coefficient D as a function of the flow velocity u when $\lambda_D = -1.99$. The upper and lower graphs show results from 2D and 3D simulations, respectively. The dots represent results from simulations whereas the solid lines show the analytic values given in Eq. (77).

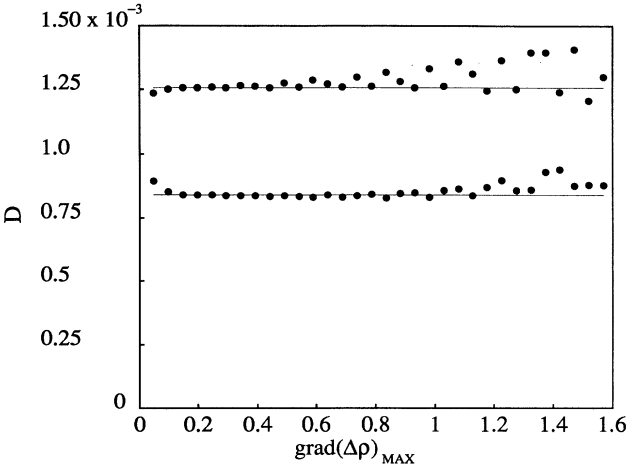

FIG. 4. The diffusion coefficient D as a function of the maximum value of the gradient of the color difference, $(\nabla\Delta\rho)_{\max}$. The upper and lower graphs show results from 2D and 3D simulations, respectively. The dots represent results from simulations whereas the solid lines show the constant analytic value.

the diffusive transport is very small. These deviations disappear when double precision is used. For the largest gradients there are only four sampling points per wavelength, and discretization effects become important. It is in fact remarkable that agreement between simulations and theory within 10% is observed even when $\Delta\rho$ is of the order unity.

CONCLUSIONS

We have developed BGK models for two-component miscible fluid flow in both 2D and 3D, and shown that they behave according to the analytic predictions. The computational performance of the models has been investigated, particularly in the regime of high Peclet numbers and large gradients in the color field. It has been confirmed that the value of the diffusion coefficient, D, obtained by measuring the relaxation of a sinusoidal concentration profile, is very close to the theoretical value, at least for diffusion coefficients greater than 10^{-4}. The corrections to the convection diffusion equation stemming from terms of higher order in u in the Chapman-Enskog expansion have been confirmed by simulations. It has been shown how the present BGK models are connected to the Boltzmann model of Holm and Rothman, and how the latter may be reduced to the former by a proper choice of eigenvalues of the collision operator. Finally, we have examined the model sensitivity to large gradients in the concentration profile, and shown that the theoretical values for the diffusion coefficient can be reproduced quite closely even when these gradients are very large.

ACKNOWLEDGMENTS

I would like to thank J. Feder and T. Jøssang for stimulating discussions and for motivating this research through their experimental work. I am also grateful

to Y. H. Qian, P. Meakin, and S. Gundersen for helpful comments. I acknowledge support by VISTA, a research cooperation between the Norwegian Academy of Science and Letters and Den norske stats oljeselskap a.s. (STATOIL) and by NAVF, the Norwegian Research Council for Science and the Humanities. Computations were done on the Connection Machine funded by the French Ministry of Education (MEN) and National Center for Scientific Research (CNRS). They could not have been done without the help of the sponsors of the Seismic Simulation Project [Amoco, CEA (French Atomic Energy Authority), Delany Enterprises Inc., Digital Equipment Corp., Elf-Aquitaine, GOCAD, Norsk Hydro, Shell, Thinking Machines Corp., Total-CFP, and Unocal].

[1] U. Frisch, B. Hasslacher, and Y. Pomeau, Phys. Rev. Lett. **56**, 1505 (1986).
[2] D. H. Rothman, Geophysics **53**, 509 (1988).
[3] C. Burges and S. Zaleski, Complex Systems **1**, 31 (1987).
[4] D. d'Humieres, P. Lallemand, J. P. Boon, D. Dab, and A. Noullez, *Proceedings of the Workshop on Chaos and Complexity*, Torino, 1987, edited by R. Livi *et al.* (World Scientific, Singapore, 1988), p. 427.
[5] D. H. Rothman and J. M. Keller, J. Stat. Phys. **52**, 1119 (1988).
[6] D. Bernardin and O. E. Sero-Guillaume, Eur. J. Mech. B **9**, 21 (1989).
[7] E. G. Flekkøy, J. Feder, and T. Jøssang, J. Stat. Phys. **68**, 515 (1992).
[8] G. R. McNamara and G. Zanetti, Phys. Rev. Lett. **61**, 2332 (1988).
[9] U. Frisch, D. d'Humieres, B. Hasslacher, P. Lallemand, Y. Pomeau, and J. P. Rivet, Complex Systems **1**, 649 (1987).
[10] F. J. Higuera and S. Succi, Europhys. Lett. **8**, 517 (1989).
[11] F. J. Higuera, S. Succi, and R. Benzi, Europhys. Lett. **9**, 345 (1989).
[12] F. J. Higuera and J. Jiménez, Europhys. Lett. **9**, 663 (1989).
[13] D. d'Humiéres and P. Lallemand, Europhys. Lett. **2**, 291 (1986).
[14] Y. H. Qian, D. d'Humiéres, and P. Lallemand, Europhys. Lett. **17**, 479 (1992).
[15] P. Bhatnagar, E. P. Gross, and M. K. Krook, Phys. Rev. **94**, 511 (1954).
[16] A. K. Gunstensen, D. H. Rothman, S. Zaleski, and G. Zanetti, Phys. Rev. A **43**, 4320 (1991).
[17] R. Holme and D. H. Rothman, J. Stat. Phys. **68**, 480 (1992).
[18] Sound waves appear when the lattice is initialized with density variations. In the following we will be concerned with the incompressible regime where the mass density is approximately constant.
[19] This definition differs from that given in Ref. [9] by the inclusion of the t_i factor. For the 3D model this factor must be present in order to obtain isotropy of $T_{\alpha\beta\gamma\delta}$.
[20] Y. H. Qian, Doctoral thesis, University of Paris 6, 1990.
[21] P. J. Davis, *Circulant Matrices* (Wiley, New York, 1979).
[22] Introducing a finite thickness of the 3D lattice in the z direction did not alter the results.